Nuclear Charge Distributions of Isotone Pairs. II. ^{39}K and ^{40}Ca†*

B. B. P. Sinha,‡ G. A. Peterson, and R. R. Whitney
Department of Physics, University of Massachusetts, Amherst, Massachusetts 01002

and

I. Sick§ and J. S. McCarthy¶
High Energy Physics Laboratory, Stanford University, Stanford, California 94305
(Received 23 February 1973)

Cross sections for electron elastic scattering from $^{39}_{19}$K and $^{40}_{20}$Ca are given for the momentum-transfer range from 0.6 to 3.4 fm^{-1}. The data were analyzed by means of a phase-shift code using phenomenological Fermi charge distributions modified with small undulations. The difference of the ^{39}K and ^{40}Ca distributions has been compared with a $1d_{3/2}$ proton distribution and with other nuclear models.

I. INTRODUCTION

We have undertaken a study of elastic electron scattering from isotones in order to learn how charge distributions change when the number of neutrons is held fixed and the number of protons is varied. In an earlier paper[1] we discussed the high-momentum-transfer elastic scattering of electrons from the isotones ^{31}P and ^{32}S, whose ground states differ primarily by a $2s_{1/2}$ proton according to the shell model. Phenomenological charge distributions were used in a distorted-wave phase-shift calculation to fit the cross sections. The difference of the ^{31}P and ^{32}S charge distributions multiplied by $4\pi r^2$, and representing a net charge of one proton, showed a concentration of charge in a large peak at about 4.0 fm and an indication of a smaller peak at about 1.2 fm, as is expected for a simple $2s_{1/2}$ proton-distribution model.

In this paper we have used the same methods to find the ground-state charge-distribution parameters of ^{39}K and ^{40}Ca. These nuclei differ by a $1d_{3/2}$ proton according to the shell model in which ^{40}Ca has closed proton and neutron shells and ^{39}K lacks a single $1d_{3/2}$ proton from having both shells closed. Corrections for elastic scattering from higher multipoles were necessary for ^{39}K, since its ground-state spin of $\frac{3}{2}$ allowed both charge-monopole and -quadrupole and magnetic-dipole and -octupole scattering. In the last section we compare our extracted charge distributions with model calculations. A preliminary report of this comparison has been given.[2]

II. MEASUREMENTS AND DATA ANALYSIS

The experiment was performed on the Stanford Mark III linear accelerator under conditions similar to those of the earlier paper,[1] hereafter referred to as (I).

The properties of the targets used are given in Table I. The C and CH_2 targets were used for the calibration of the spectrometer detector system. Estimates of the effects on the ^{39}K cross section of the ^{41}K present in its natural percentage abundance in the K target showed that they were always less than the statistical uncertainties of the cross sections, and therefore they were not taken into account. The contribution of small oxygen impurities in the ^{39}K and ^{40}Ca targets were subtracted after measuring the small recoil-displaced oxygen peak cross sections at one momentum transfer and then normalizing calculated oxygen cross sections to them. An oxygen charge distribution obtained from the experimental results of Sick and McCarthy[3] was used in a phase-shift code[4] to calculate the oxygen cross sections.

Data corrections similar to those in (I) were made. As mentioned in (I), several calibrations

TABLE I. Target data.

Target	Runs	Thickness (mg/cm^2)	Isotopic abundance	Isotopic impurity
^{39}K	249.3 and 496.8 MeV	400 ± 8	Natural 93.22%	6.77% ^{41}K
^{39}K	150 MeV	100 ± 2	Natural 93.22%	6.77% ^{41}K
^{40}Ca	All	505 ± 10	Enriched 99.97%	
CH_2	All	672 ± 5	···	
^{12}C	All	480 ± 5	Natural 98.89%	1.11% ^{13}C

made since the ^{40}Ca studies of Frosch *et al.*[5] and of Bellicard *et al.*[6] led to improved accuracies in the cross sections. For this experiment the incident energies were known to ±0.1%, the central scattering angle to ±0.03°, and the incoming beam direction to ±0.02°. The experimental cross sections were averaged over the spectrometer acceptance angle of ±0.93° and are given in Tables II and III as a function of the central scattering angle for center-of-target energies of 150.0, 249.3, and 496.8 MeV, corresponding to a momentum-transfer range from 0.6 to 3.4 fm^{-1}. Additional ^{40}Ca data from other experiments are also included. A 3% systematic error has to be added to all data of this experiment.

The phase-shift code[4,7] used in this study calculates the scattering only from a charge monopole and does not calculate the scattering from higher multipole moments. Calculations of the charge monopole scattering from spinless ^{40}Ca were made directly for specific static-charge-distribution models with this code. However, in the case of ^{39}K, it was necessary to estimate and subtract the small scattering contributions due to higher multi-

TABLE II. Experimental results for ^{39}K. The differential cross sections and their errors are in the laboratory frame in units of millibarns per steradian.

Angle (deg)	Cross section (mb/sr)	Error (mb/sr)	Angle (deg)	Cross section (mb/sr)	Error (mb/sr)
	150.0 MeV			249.3 MeV *(Continued)*	
50.00	0.364	0.32×10^{-2}	82.00	0.397×10^{-4}	0.13×10^{-5}
55.00	0.163	0.12×10^{-2}	84.00	0.273×10^{-4}	0.98×10^{-6}
60.00	0.710×10^{-1}	0.90×10^{-3}	86.00	0.183×10^{-4}	0.40×10^{-6}
65.00	0.303×10^{-1}	0.10×10^{-3}	88.00	0.116×10^{-4}	0.32×10^{-6}
70.00	0.124×10^{-1}	0.40×10^{-4}	90.00	0.699×10^{-5}	0.28×10^{-6}
75.00	0.481×10^{-1}	0.27×10^{-4}	92.00	0.406×10^{-5}	0.26×10^{-6}
80.00	0.171×10^{-1}	0.16×10^{-4}	94.00	0.225×10^{-5}	0.14×10^{-6}
85.00	0.564×10^{-3}	0.89×10^{-5}	96.00	0.126×10^{-5}	0.98×10^{-7}
90.00	0.193×10^{-3}	0.53×10^{-5}	98.00	0.638×10^{-6}	0.62×10^{-7}
95.00	0.957×10^{-4}	0.25×10^{-5}	100.00	0.421×10^{-6}	0.51×10^{-7}
100.00	0.821×10^{-4}	0.34×10^{-5}	104.00	0.171×10^{-6}	0.25×10^{-7}
105.00	0.833×10^{-4}	0.36×10^{-5}	107.00	0.258×10^{-6}	0.28×10^{-7}
110.00	0.808×10^{-4}	0.42×10^{-5}	110.00	0.301×10^{-6}	0.29×10^{-7}
115.00	0.717×10^{-4}	0.44×10^{-5}			
	249.3 MeV			496.8 MeV	
34.00	0.349	0.37×10^{-2}	34.00	0.109×10^{-2}	0.26×10^{-4}
36.00	0.191	0.26×10^{-2}	36.00	0.653×10^{-3}	0.15×10^{-4}
38.00	0.110	0.16×10^{-2}	38.00	0.338×10^{-3}	0.10×10^{-4}
40.00	0.580×10^{-1}	0.64×10^{-3}	40.00	0.137×10^{-3}	0.58×10^{-5}
42.00	0.312×10^{-1}	0.44×10^{-3}	42.00	0.475×10^{-4}	0.23×10^{-5}
44.00	0.162×10^{-1}	0.21×10^{-3}	44.00	0.141×10^{-4}	0.95×10^{-6}
46.00	0.747×10^{-2}	0.11×10^{-3}	46.00	0.280×10^{-5}	0.15×10^{-6}
48.00	0.337×10^{-2}	0.40×10^{-4}	47.10	0.148×10^{-5}	0.12×10^{-6}
50.00	0.153×10^{-2}	0.19×10^{-4}	48.00	0.166×10^{-5}	0.99×10^{-7}
52.00	0.772×10^{-3}	0.12×10^{-4}	50.00	0.277×10^{-5}	0.15×10^{-6}
53.00	0.580×10^{-3}	0.32×10^{-5}	52.00	0.345×10^{-5}	0.14×10^{-6}
54.00	0.442×10^{-3}	0.69×10^{-5}	54.00	0.292×10^{-5}	0.13×10^{-6}
55.00	0.425×10^{-3}	0.65×10^{-5}	56.00	0.226×10^{-5}	0.15×10^{-6}
56.00	0.409×10^{-3}	0.63×10^{-5}	58.00	0.146×10^{-5}	0.86×10^{-7}
58.00	0.412×10^{-3}	0.68×10^{-5}	60.00	0.760×10^{-6}	0.56×10^{-7}
60.00	0.422×10^{-3}	0.58×10^{-5}	62.00	0.475×10^{-6}	0.33×10^{-7}
62.00	0.410×10^{-3}	0.61×10^{-5}	64.00	0.227×10^{-6}	0.24×10^{-7}
64.00	0.365×10^{-3}	0.55×10^{-5}	66.00	0.101×10^{-6}	0.14×10^{-7}
66.00	0.324×10^{-3}	0.46×10^{-5}	68.00	0.440×10^{-7}	0.81×10^{-8}
68.00	0.276×10^{-3}	0.42×10^{-5}	70.00	0.183×10^{-7}	0.44×10^{-8}
70.00	0.233×10^{-3}	0.36×10^{-5}	72.00	0.116×10^{-7}	0.31×10^{-8}
72.00	0.183×10^{-3}	0.30×10^{-5}	74.00	0.55×10^{-8}	0.23×10^{-8}
74.00	0.144×10^{-3}	0.26×10^{-5}	76.00	0.29×10^{-8}	0.11×10^{-8}
76.00	0.108×10^{-3}	0.19×10^{-5}	78.00	0.30×10^{-8}	0.15×10^{-8}
78.00	0.779×10^{-4}	0.16×10^{-5}	80.00	0.25×10^{-8}	0.13×10^{-8}
80.00	0.584×10^{-4}	0.14×10^{-5}	83.00	0.13×10^{-8}	0.74×10^{-9}
			86.00	0.89×10^{-9}	0.63×10^{-9}

TABLE III. Experimental results for ^{40}Ca. The differential cross sections and their errors are in the laboratory frame in units of millibarns per steradian.

Angle (deg)	Cross section (mb/sr)	Error (mb/sr)
This experiment 249.3 MeV		
40.00	0.577×10^{-1}	0.61×10^{-3}
46.00	0.648×10^{-2}	0.92×10^{-4}
52.00	0.730×10^{-3}	0.11×10^{-4}
54.00	0.532×10^{-3}	0.67×10^{-5}
58.00	0.526×10^{-3}	0.81×10^{-5}
66.00	0.405×10^{-3}	0.59×10^{-5}
72.00	0.204×10^{-3}	0.30×10^{-5}
76.00	0.110×10^{-3}	0.19×10^{-5}
82.00	0.360×10^{-4}	0.12×10^{-5}
92.00	0.287×10^{-5}	0.12×10^{-6}
Previous experiment A [a] 249.3 MeV		
24.08	0.527×10	0.15
26.08	0.312×10	0.10
28.08	0.181×10	0.61×10^{-1}
30.08	0.106×10	0.34×10^{-1}
32.08	0.614	0.20×10^{-1}
34.08	0.340	0.11×10^{-1}
36.08	0.199	0.61×10^{-2}
38.08	0.107	0.34×10^{-2}
40.08	0.557×10^{-1}	0.17×10^{-2}
42.08	0.284×10^{-1}	0.92×10^{-3}
44.08	0.149×10^{-1}	0.48×10^{-3}
46.08	0.702×10^{-2}	0.22×10^{-3}
48.08	0.316×10^{-2}	0.91×10^{-4}
50.08	0.143×10^{-2}	0.45×10^{-4}
52.08	0.741×10^{-3}	0.22×10^{-4}
54.08	0.562×10^{-3}	0.17×10^{-4}
56.08	0.518×10^{-3}	0.16×10^{-4}
58.08	0.549×10^{-3}	0.17×10^{-4}
60.08	0.545×10^{-3}	0.17×10^{-4}
62.08	0.516×10^{-3}	0.16×10^{-4}
64.08	0.465×10^{-3}	0.15×10^{-4}
66.08	0.397×10^{-3}	0.13×10^{-4}
68.08	0.326×10^{-3}	0.10×10^{-4}
70.08	0.262×10^{-3}	0.85×10^{-5}
72.08	0.202×10^{-3}	0.66×10^{-5}
74.08	0.152×10^{-3}	0.36×10^{-5}
76.08	0.114×10^{-3}	0.36×10^{-5}
78.08	0.800×10^{-4}	0.23×10^{-5}
80.08	0.550×10^{-4}	0.15×10^{-5}
82.08	0.376×10^{-4}	0.11×10^{-5}
84.08	0.241×10^{-4}	0.76×10^{-6}
86.08	0.153×10^{-4}	0.49×10^{-6}
88.08	0.918×10^{-5}	0.31×10^{-6}
90.08	0.559×10^{-5}	0.22×10^{-6}
Previous experiment B [a] 249.3 MeV		
26.08	0.297×10	0.41×10^{-1}
32.08	0.579	0.80×10^{-2}
34.08	0.335	0.53×10^{-2}
36.07	0.188	0.31×10^{-2}
38.07	0.100	0.16×10^{-2}
40.07	0.549×10^{-1}	0.82×10^{-3}
42.07	0.267×10^{-1}	0.39×10^{-3}
46.06	0.614×10^{-2}	0.91×10^{-4}
50.06	0.127×10^{-2}	0.12×10^{-4}
52.06	0.714×10^{-3}	0.14×10^{-4}
54.06	0.523×10^{-3}	0.78×10^{-5}
56.06	0.496×10^{-3}	0.62×10^{-5}
60.05	0.512×10^{-3}	0.79×10^{-5}
62.05	0.495×10^{-3}	0.79×10^{-5}
64.05	0.424×10^{-3}	0.79×10^{-5}
66.05	0.392×10^{-3}	0.62×10^{-5}
70.05	0.257×10^{-3}	0.41×10^{-5}
74.05	0.148×10^{-3}	0.25×10^{-5}
76.04	0.104×10^{-3}	0.18×10^{-5}
80.05	0.531×10^{-4}	0.11×10^{-5}
84.05	0.234×10^{-4}	0.50×10^{-6}
90.06	0.528×10^{-5}	0.14×10^{-6}
94.06	0.138×10^{-5}	0.49×10^{-7}
100.06	0.226×10^{-6}	0.25×10^{-7}
This experiment 496.8 MeV		
34.00	0.119×10^{-2}	0.18×10^{-4}
40.00	0.139×10^{-3}	0.44×10^{-5}
42.00	0.405×10^{-4}	0.20×10^{-5}
48.00	0.236×10^{-5}	0.90×10^{-7}
54.00	0.322×10^{-5}	0.11×10^{-6}
63.00	0.279×10^{-6}	0.24×10^{-7}
66.00	0.673×10^{-7}	0.89×10^{-8}
69.00	0.161×10^{-7}	0.49×10^{-8}
80.00	0.220×10^{-8}	0.13×10^{-8}
Previous experiment C [a] 496.8 MeV		
20.16	0.218	0.62×10^{-2}
21.16	0.115	0.32×10^{-2}
22.16	0.561×10^{-1}	0.19×10^{-2}
23.16	0.256×10^{-1}	0.82×10^{-3}
24.16	0.111×10^{-1}	0.36×10^{-3}
25.16	0.533×10^{-2}	0.18×10^{-3}
26.16	0.296×10^{-2}	0.10×10^{-3}
27.94	0.192×10^{-2}	0.81×10^{-4}
28.94	0.213×10^{-2}	0.83×10^{-4}
29.94	0.218×10^{-2}	0.83×10^{-4}
31.93	0.187×10^{-2}	0.82×10^{-4}
33.21	0.146×10^{-2}	0.53×10^{-4}
34.22	0.117×10^{-2}	0.41×10^{-4}
35.21	0.901×10^{-3}	0.26×10^{-4}
36.21	0.670×10^{-3}	0.25×10^{-4}
37.22	0.466×10^{-3}	0.21×10^{-4}
38.22	0.322×10^{-3}	0.13×10^{-4}
39.23	0.203×10^{-3}	0.83×10^{-5}
40.26	0.124×10^{-3}	0.51×10^{-5}
40.26	0.118×10^{-3}	0.51×10^{-5}
41.27	0.720×10^{-4}	0.33×10^{-5}
42.74	0.273×10^{-4}	0.12×10^{-5}
43.28	0.188×10^{-4}	0.82×10^{-6}
44.23	0.910×10^{-4}	0.41×10^{-6}
45.28	0.436×10^{-5}	0.21×10^{-6}
46.17	0.238×10^{-5}	0.10×10^{-6}
47.24	0.209×10^{-5}	0.81×10^{-7}
50.26	0.345×10^{-5}	0.15×10^{-6}
52.26	0.356×10^{-5}	0.16×10^{-6}

Previous experiment B [a] 249.3 MeV *(Continued)*

TABLE III *(Continued)*

Angle (deg)	Cross section (mb/sr)	Error (mb/sr)	Angle (deg)	Cross section (mb/sr)	Error (mb/sr)
Previous experiment C [a] 496.8 MeV *(Continued)*			Previous experiment 757.5 MeV [b] *(Continued)*		
54.26	0.290×10^{-5}	0.14×10^{-6}	42.08	0.285×10^{-6}	0.65×10^{-7}
56.00	0.212×10^{-5}	0.92×10^{-7}	44.08	0.450×10^{-7}	0.16×10^{-7}
58.00	0.151×10^{-5}	0.82×10^{-7}	45.08	0.260×10^{-7}	0.60×10^{-8}
60.00	0.871×10^{-6}	0.46×10^{-7}	46.08	0.190×10^{-7}	0.60×10^{-8}
Previous experiment 757.5 MeV [b]			47.08	0.560×10^{-8}	0.14×10^{-8}
			48.08	0.420×10^{-8}	0.20×10^{-8}
31.08	0.510×10^{-5}	0.80×10^{-6}	49.08	0.395×10^{-8}	0.17×10^{-8}
32.08	0.780×10^{-5}	0.11×10^{-6}	50.08	0.640×10^{-8}	0.31×10^{-8}
34.08	0.890×10^{-5}	0.11×10^{-6}	52.08	0.480×10^{-8}	0.20×10^{-8}
36.08	0.630×10^{-5}	0.80×10^{-6}			
38.08	0.280×10^{-5}	0.40×10^{-6}			
40.08	0.110×10^{-5}	0.30×10^{-6}			

[a] The previously unpublished data sets indicated as Previous experiments A, B, and C were taken at a time preceding the ^{39}K data by J. Heisenberg, J. McCarthy, and I. Sick.
[b] The 757.5-MeV data are those of Bellicard *et al.* (Ref. 6).

poles from the experimental cross sections in order to obtain the dominant charge-monopole cross section. The form factors, $F(q)$, for higher moments in ^{39}K were calculated as a function of the momentum transfer, q, in the plane-wave first-Born approximation by Walker,[8,9] who assumed that the moments are due to a single $d_{3/2}$ proton hole moving in a harmonic-oscillator potential well of ^{40}Ca. As in (I), experimental estimates of higher multipole contributions were obtained by making a crude separation of longitudinal (charge) and transverse (current and magnetic) contributions for $q^2 \simeq 4.0$ fm^{-2}. The calculated magnetic contributions were scaled in the same manner as the ^{31}P results of (I) were scaled to the experimentally measured magnetic contributions. The higher multipole contributions were small ($\lesssim 1\%$) compared to those of the charge monopole, except for a few large-angle cases, and for regions near the charge-monopole diffraction minima. The largest contributions were about $(17 \pm 6)\%$ of the corresponding experimental contribution at 496.8 MeV and $\theta \simeq 47.1°$, a diffraction minimum, and $(34 \pm 10)\%$ at 249.3 MeV and $\theta \simeq 104°$, as shown in Table IV.

The 150-MeV data and the 249.3-MeV data could be fitted by using the parabolic Fermi charge distribution

$$\rho(r) = \rho_0(1 + wr^2/c^2)(1 + e^{(r-c)/z})^{-1}, \quad (1)$$

where ρ_0 is a normalization constant, and c, z, and w are three adjustable parameters. The 496.8-MeV data required the addition to Eq. (1) of a modulation $\Delta\rho(r)$ so that $\rho(r)$ took a form similar to the one described by Bellicard *et al.*,[6]

$$\rho(r) = \rho_0\left[\frac{1 + w(r/c)^2}{1 + e^{(r-c)/z}} + A'\frac{\sin q_0 r}{q_0 r}\, e^{-p_0^2 r^2/4}\right], \quad (2)$$

TABLE IV. Calculated higher multipole contributions for ^{39}K in percent of the experimental cross sections of Table II.

150 MeV				249.3 MeV				496.8 MeV			
θ (deg)	$M1$ (%)	$M3$ (%)	$E2$ (%)	θ (deg)	$M1$ (%)	$M3$ (%)	$E2$ (%)	θ (deg)	$M1$ (%)	$M3$ (%)	$E2$ (%)
50	0.003	0.000	0.031	38	0.033	0.003	0.13	34	0.024	0.510	0.096
55	0.005	0.001	0.043	46	0.071	0.048	0.04	42	0.043	2.120	0.089
60	0.010	0.002	0.062	54	0.31	0.73	1.13	47.1	1.050	14.990	1.44
65	0.004	0.018	0.088	60	0.09	0.59	0.26	50	0.410	4.110	0.550
70	0.034	0.012	0.126	70	0.006	0.57	0.01	54	0.130	0.800	0.120
80	0.140	0.101	0.304	80	0.005	1.05	0.004	60	0.075	0.310	0.042
90	0.715	0.977	0.919	86	0.042	1.88	0.023	64	0.066	0.260	0.032
100	0.970	2.211	0.628	92	0.21	4.90	0.09	68	0.092	0.310	0.032
105	0.776	2.089	0.336	96	0.61	10.65	0.20	72	0.054	0.160	0.015
110	0.624	2.051	0.183	104	2.59	31.30	0.53	76	0.030	0.081	0.005
115	0.579	2.184	0.110	110	1.44	15.74	0.21	86	0.002	0.010	0.000

TABLE V. Charge-distribution best-fit parameters. Numerical values for ^{39}K and ^{40}Ca of the best-fit parameters of the parabolic Fermi charge distribution with an additional oscillatory term as given by Eq. (2).

	^{39}K	^{40}Ca
c (fm)	3.743 ± 0.025	3.766 ± 0.023
z (fm)	0.585 ± 0.006	0.586 ± 0.005
w	−0.201 ± 0.022	−0.161 ± 0.023
q_0 (fm^{-1})	3.14 ± 0.06	3.14 ± 0.05
p_0 (fm^{-1})	0.43 ± 0.04	0.43 ± 0.04
A'	0.086 ± 0.007	0.0814 ± 0.008
$\langle r^2\rangle^{1/2}$ (fm)	3.408 ± 0.027	3.482 ± 0.025

where A', p_0, and q_0 are additional adjustable parameters.

All of the parameters were varied until a best fit was obtained as indicated by the lowest χ^2 in the comparison of the measured differential cross sections and the calculated ones folded with the acceptance angle of the spectrometer. The correlated errors for all of the fitting parameters were determined by finding a variation of unity in the χ^2 surface representing the fits to the data using the parameters. Parameter errors arising from the ±3% uncertainty in the hydrogen calibration and the ±2% target thickness uncertainties were found by refitting the data after shifting it to account for these systematic errors. These latter parameter errors were then added to the correlated parameter errors.

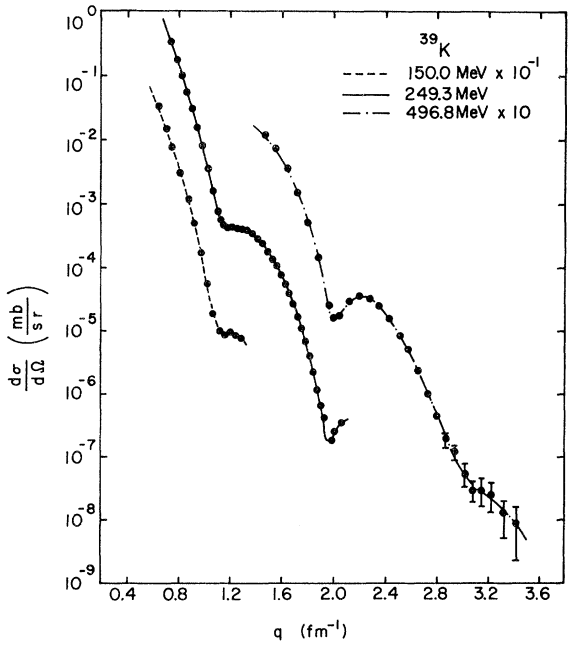

FIG. 1. Experimental cross sections for the elastic scattering of 150.0-, 249.3-, and 496.8-MeV electrons from ^{39}K versus momentum transfer.

All data, including those indicated as previous experiments A, B, and C of Table III, and the 757.5-MeV data of Bellicard *et al.*[6] could be fitted by using Eq. (2) with the parameters indicated in Table V. For the ^{40}Ca data, a χ^2 of 154 for 119 degrees of freedom, and for ^{39}K, a χ^2 of 70.4 for 74 degrees of freedom, were obtained. The best-fit calculated cross-section curves are shown in Figs. 1 and 2, and the corresponding charge distributions in Figs. 3 and 4.

III. RESULTS AND DISCUSSION

For ^{40}Ca the parameter z agrees closely with the 250-MeV results of Frosch *et al.*,[5] as does our rms radius of 3.482 ± 0.025 fm, but our values of c and w, the two most strongly correlated parameters, differ somewhat. The charge modification parameters p_0 and q_0 of ^{40}Ca are in agreement with those of Bellicard *et al.*[6] The ^{39}K rms charge radius of 3.408 ± 0.027 fm is in good agreement with the muonic x-ray result, 3.44 ± 0.03 fm, which we extracted from the $2p$-$1s$ energies given by Wu and Willets,[10] after correcting them for nuclear polarization.[11] For these isotones we find a variation

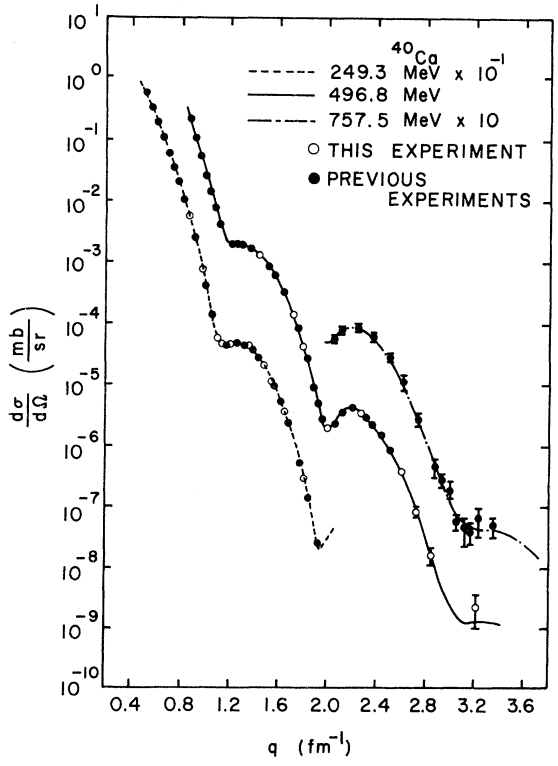

FIG. 2. Experimental cross sections for the elastic scattering from ^{40}Ca of 249.3-, 496.8-, and 757.5-MeV electrons versus momentum transfer. Some of the data are not of this experiment. See Table III for references.

in $\langle r^2 \rangle^{1/2}$ greater than their variation in $A^{1/3}$ by 1.3%, in contrast to the isotopes[5] of Ca where it is less than $A^{1/3}$. This is in agreement with Elton's conclusions about nuclear compressibility.[12]

Shown in Figs. 3 and 4 are the results of shell-model calculations by Gerace and Hamilton[13] of the charge densities of ^{39}K and ^{40}Ca. The Woods-Saxon well parameters were separately adjusted for s and d states and for p states to fit the rms radii, and the known separation energies as given by $(p, 2p)$, (γ, n), and (γ, p) experiments for the $2s_{1/2}$, $1d_{5/2}$, and $1d_{3/2}$ particles, and separation energy estimates for the $1s_{1/2}$, $1p_{3/2}$, and $1p_{1/2}$ particles. The $1s_{1/2}$ separation energy was lowered so that the same s-d well could be used for all s and d particles. Also a 0.8-fm-rms-radius Gaussian proton distribution was folded into the distribution of proton centers. As can be seen in Figs. 3 and 4, the small undulations in the shell-model charge density also appear in the phenomenological charge distribution as given by Eq. (2) with the experimentally determined best-fit parameters of Table V.

In Fig. 5 is shown the difference between the ^{40}Ca and the ^{39}K phenomenological charge distributions multiplied by $4\pi r^2$, a quantity better determined by electron scattering experiments than the charge density difference itself. The error bars shown in Fig. 5 are based entirely upon the errors in the parameters c, z, and w as determined by finding a variation of unity in the χ^2 surface representing the fits to the data using these parameters. The parameters c, z, and w were allowed to take on all combinations to the full ranges of their uncertainties as calculated in the χ^2 analysis, consistent with the rms radius not exceeding its uncertainty, as well as allowing for the 2% target-thickness errors. In this manner the errors in the two charge densities were found and then added together for the difference curves. The resulting errors are shown centered around the difference of three-parameter distributions. The values of c, z, and w used in the three-parameter distributions are the same as those of Table V. It can be seen that there is little difference between the six-parameter charge-density difference curve and the three-parameter one. The shape of the difference curve is determined primarily by the low-q data.

The small negative portion of the curve within 2.1 fm, although certainly small compared with the errors, could represent the amount of charge displaced outward due to Coulomb repulsion, as well as changes in the width and depth of the nu-

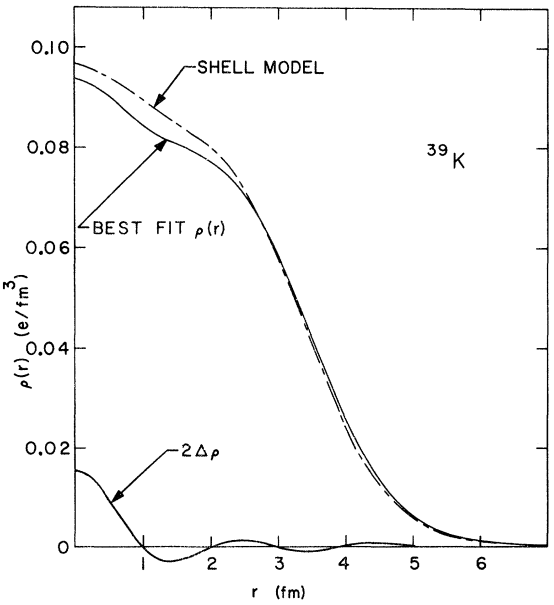

FIG. 3 The charge distribution of ^{39}K. The curve labeled "shell model" is the result of a calculation using a Woods-Saxon potential well. The solid curve is the six-parameter distribution of Eq. (2) with the best-fit parameters obtained by simultaneously fitting all of the data of Fig. 1. The lower solid curve is twice the oscillatory second term of Eq. (2).

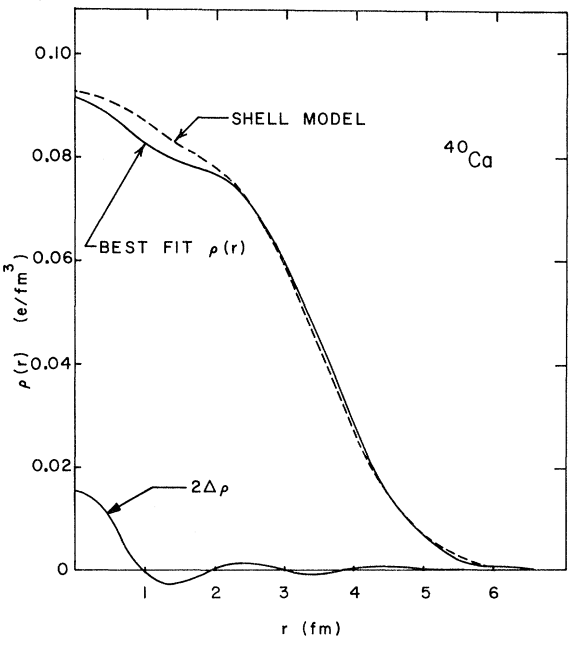

FIG. 4. The charge distribution of ^{40}Ca. The curve labeled "shell model" is the result of a calculation using a Woods-Saxon potential well. The solid curve is the six-parameter distribution of Eq. (2) with the best-fit parameters obtained by simultaneously fitting all of the data of Fig. 2. The lower solid curve is twice the oscillatory second term of Eq. (2).

clear central potential resulting from the influence of the added proton on the ^{39}K core.

The major portion of the difference curve in Fig. 5 lies beyond 2.1 fm and represents mainly the last $d_{3/2}$ proton in ^{40}Ca. This can be seen in Fig. 6 where the single-particle shell-model calculations of Gerace and Hamilton[13] are shown with the experimental errors superimposed. The harmonic-oscillator density shown was generated by using length parameters which reproduced correct rms radii. The Woods-Saxon density difference was calculated as indicated above.

It can be seen from Fig. 6 that both the harmonic-oscillator and the Woods-Saxon models can satisfactorily account for the charge-density differences. Thus although the shell model did not correctly predict the total densities for ^{39}K and ^{40}Ca, as shown in Figs. 3 and 4, it can explain the relative charge densities of these two nuclei by using the experimental information on the relatively large difference between the rms radii.

Figure 7 shows the charge-density difference obtained from a different approach, the Hartree-Fock (HF) calculations of Giai and Vénéroni,[14] in which no experimental data specific to ^{39}K or ^{40}Ca are used. Instead these calculations are based upon the use of the Skyrme interaction[15] force (I) whose parameters have been determined by fits to rms radii and single-particle energies over the whole Periodic Table. Also shown in Fig. 7 is the charge density of a $d_{3/2}$ proton as given by an HF wave function with folded proton size. The experimental charge density difference is not explained by either result. The difference between the HF density difference and the $d_{3/2}$ proton density is due to the influence of the added proton on the ^{39}K core. The fact that the experimental difference peaks at a larger radius indicates that the wave function

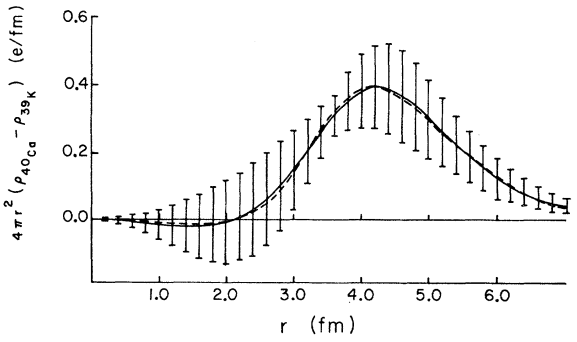

FIG. 5. The difference between the phenomenological best-fit charge distributions of ^{40}Ca and ^{39}K multiplied by $4\pi r^2$ for the three-parameter distributions of Eq. (1) (solid curve) and for the six-parameter distributions of Eq. (2) (dashed curve). The error bars are based entirely upon the errors in c, z and w.

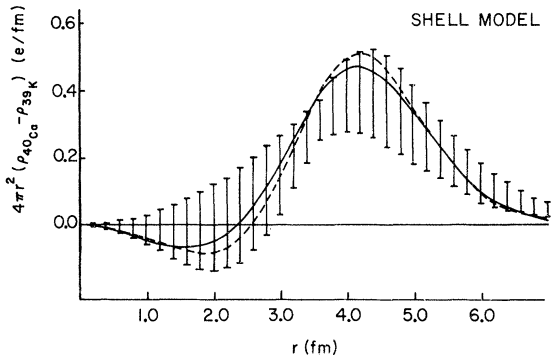

FIG. 6. The difference between the shell-model charge distributions of ^{40}Ca and ^{39}K multiplied by $4\pi r^2$ which were calculated by using the harmonic-oscillator approximation (solid curve) and by using the Woods-Saxon well parameters of Ref. 13 (dashed curve). The error bars are those of Fig. 5.

changes more when adding the $d_{3/2}$ proton than can be accounted for by HF. This may be interpreted as a rearrangement effect, caused by changes in the nuclear potential well due to the added proton, and possibly by configuration mixings which have not been taken into account in the HF calculation. Similar calculations[16] recently have been carried out for ^{208}Pb and ^{209}Bi in order to determine the influence of the additional proton in polarizing the doubly magic Pb core.

Some qualifying remarks are in order about our interpretation of the data. The simultaneous fitting of the data of this elastic scattering experiment ignored possible energy-dependent effects such as virtual nuclear excitations, wherein a nucleus is raised to an excited state by the absorption of a virtual photon while making a transition to the ground state via a second exchanged

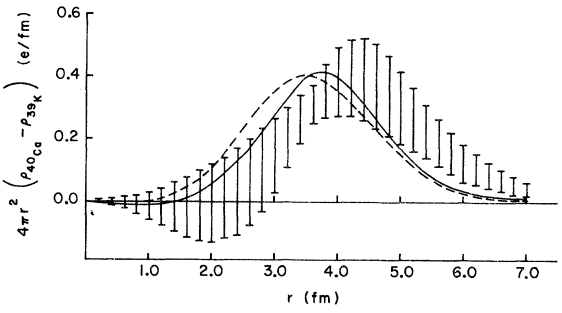

FIG. 7. The difference between Hartree-Fock charge distributions of ^{40}Ca and ^{39}K multiplied by $4\pi r^2$ (solid curve), and the charge distribution of a Hartree-Fock $d_{3/2}$ proton multiplied by $4\pi r^2$ (dashed curve). The experimental error bars are those of Fig. 6.

virtual photon. Lin[17] has estimated that such effects are of the order of 3%. Their estimated small size justifies their omission in this experiment. They should be included in more accurate experiments of the future. We took the conventional approach of assuming a model for a static charge distribution and then determined its parameters by a fit to all data simultaneously. The uncertainties in our extracted charge distributions should be interpreted only in the context of the assumed phenomenological model given by Eq. (2). Model-independent analysis[18] of elastic scattering could yield larger charge-distribution uncertainties than we have found in our results.

In our analysis c, z, and w were not assumed to be determined by low-q data and then held fixed while the high-q data were fitted by the variation of the three additional parameters of Eq. (2), as has sometimes been done. Rather all six parameters of Eq. (2) were varied simultaneously. This approach removes the ambiguity of setting an arbitrary boundary between low- and high-q data. The parameters c, z, and w will have different values depending upon where this boundary is set. For example, in the case of fitting simultaneously six parameters to the high-q 496.8-MeV ^{40}Ca data, the c, z, and w parameters varied by much more than their errors as calculated with the low-q 249.3-MeV data. This was not the case for ^{39}K with relatively fewer data points than ^{40}Ca. Also with the changes in c, z, and w produced by the inclusion of the high-q ^{40}Ca data, the rms radius also changed from the low-q value of 3.47 fm. Fixing the rms radius at 3.47 fm did not allow an adequate fit to the data in the high-q region.

A small ambiguity in our analysis results because the modulations added to the three-parameter Fermi distribution of Eq. (1) produce negative densities at large radii. Depending on whether the negative values are set equal to zero, and where the radial integration is cut off, resulting rms radii may vary by as much as 0.01 fm. In our difference curves of Figs. 5 and 6, the major experimental errors come from uncertainties in the rms radii of ^{39}K and ^{40}Ca.

Recently it has been proposed[19] that neutrons can make substantial contributions to elastic electron scattering because of their distributed charge and their spin-orbit interaction in spin unsaturated shells. In the case of both ^{39}K and ^{40}Ca, with closed s-d neutron shells, only the charge distribution of the individual neutrons gives a scattering contribution. Since the number of neutrons is the same in any isotone pair, it is understandable that isotone charge differences can be predicted by the shell model.

Future isotone studies call for an improvement in experimental accuracy, better measurement of magnetic contributions, better calibrations, and in addition, an improvement in analysis.

ACKNOWLEDGMENTS

We wish to thank Professor W. Gerace for his help and advice pertaining to this work. Two of us (B.B.P.S. and G.A.P.) wish to thank Professor Hofstadter and Professor Yearian and their staff for the opportunity to perform this experiment at Stanford.

---

†Part of this work was submitted by B. B. P. Sinha to the faculty of the University of Massachusetts in partial fulfillment of the requirement for the degree of Doctor of Philosophy.

*Work supported in part by grants from the National Science Foundation, the Office of Naval Research, and the Research Council of the University of Massachusetts.

‡Present address: Department of Physics, University of Guelph, Guelph, Ontario, Canada.

§Present address: Physikalisches Institut, 4000 Basel, Switzerland.

¶Present address: Department of Physics, University of Virginia, Charlottesville, Virginia 22903.

[1]B. B. P. Sinha, G. A. Peterson, G. C. Li, and R. R. Whitney, Phys. Rev. C 6, 1657 (1972).

[2]B. B. P. Sinha, G. A. Peterson, I. Sick, and J. S. McCarthy, Phys. Letters 35B, 217 (1971).

[3]I. Sick and J. S. McCarthy, Nucl. Phys. A150, 631 (1970).

[4]J. Heisenberg, private communication.

[5]R. F. Frosch, R. Hofstadter, J. S. McCarthy, G. K. Nöldeke, K. J. van Oostrum, M. R. Yearian, B. C. Clark, R. Herman, and D. G. Ravenhall, Phys. Rev. 174, 1380 (1968).

[6]J. B. Bellicard, P. Bounin, R. F. Frosch, R. Hofstadter, J. S. McCarthy, B. C. Clark, R. Herman, and D. G. Ravenhall, Phys. Rev. Letters 19, 527 (1967).

[7]B. B. P. Sinha, Ph.D. thesis, University of Massachusetts at Amherst, 1971 (unpublished).

[8]G. E. Walker, private communication.

[9]T. A. Griffy and D. U. Yu, Phys. Rev. 139, B880 (1965).

[10]C. S. Wu and L. Willets, Ann. Rev. Nucl. Sci. 19, 527 (1969).

[11]M.-Y. Chen, Phys. Rev. C 1, 1167 (1970).

[12]L. R. B. Elton, Phys. Rev. 158, 970 (1967).

[13]W. J. Gerace and G. C. Hamilton, Phys. Letters 39B, 481 (1972).

[14]N. V. Giai and M. Vénéroni, Orsay, France, private communication.

[15]D. Vautherin and D. M. Brink, Phys. Rev. C 5, 626 (1972).

[16]I. Sick, H. Flocard, and M. Vénéroni, Phys. Letters 39B, 443 (1972).

[17]W. -F. Lin, Phys. Letters 39B, 447 (1972).
[18]J. Friedrich and F. Lenz, Nucl. Phys. A183, 523 (1972).
[19]W. Bertozzi, J. Friar, J. Heisenberg, and J. W. Negele, Phys. Letters 41B, 477 (1972).

PHYSICAL REVIEW C VOLUME 7, NUMBER 5 MAY 1973

Scattering of 139-MeV Alpha Particles by ^{58}Ni and ^{208}Pb†

D. A. Goldberg, S. M. Smith, H. G. Pugh, P. G. Roos, and N. S. Wall
Department of Physics and Astronomy, University of Maryland, College Park, Maryland 20742
(Received 18 December 1972)

The elastic and inelastic scattering of α particles by ^{58}Ni and ^{208}Pb has been investigated at an incident energy of 139 MeV. The elastic cross sections have been analyzed in terms of the optical model using a six-parameter Woods-Saxon potential. The data for ^{58}Ni are sufficient to eliminate the discrete ambiguity in the strength of the potential; the single potential which fits the data has a well depth of 116 MeV and a volume integral $J/4A$ of 298 MeV fm^3. For ^{208}Pb the discrete ambiguity could not be resolved. This outcome is consistent with recently developed criteria for experimental data necessary to resolve the discrete ambiguity. A discussion of the discrete ambiguity, in particular the A dependence, is given, and it is shown that measurements at higher energies are required to resolve the ambiguity for ^{208}Pb. The inelastic cross sections for transitions to the 1.45-MeV ($J^\pi = 2^+$), 2.46-MeV (4^+), 4.47-MeV (3^-) states in ^{58}Ni and the 2.62-MeV (3^-) state in ^{208}Pb have been analyzed with distorted-wave Born-approximation (DWBA) calculations using collective-model form factors. The results are consistent with previous analyses of lower-energy data.

I. INTRODUCTION

Although the study of α-particle scattering has a long history, only recently have such investigations been performed at energies above 100 MeV. Several systematic studies have now been made at 104[1] and 166 MeV.[2] We have extended these investigations by examining the elastic and inelastic scattering of α particles by ^{58}Ni and ^{208}Pb at 139 MeV.

Elastic scattering data are conventionally analyzed in terms of the optical model. Since such analyses provide a convenient avenue for obtaining scattering wave functions, the extraction of optical potentials from elastic scattering data is generally the first step in extracting nuclear structure information from other reactions involving an elastic α channel. Unfortunately, the ability to extract such information, for example, spectroscopic strengths from (^{3}He, α) reactions,[3] has been somewhat hampered at lower energies by the well-known ambiguities[4] in the α optical potential parameters. Investigations seeking information directly from the elastic scattering results, such as those attempting to determine nuclear matter distributions directly from comparisons between phenomenological and microscopic α optical potentials,[5] have likewise been hampered.

Some evidence that one might be able to resolve the discrete ambiguities using higher incident energies appears in the studies referred to above.[1,2] In addition an analysis by Duhm[6] of the elastic scattering of 119-MeV α particles by ^{24}Mg indicates no discrete ambiguity. It was therefore felt that additional investigations at higher energies might yield unambiguous results, and therefore provide information on the systematics of intermediate energy elastic scattering. It was also hoped that such investigations might lead to a better understanding of the discrete ambiguity and perhaps the means for removing it as well. The present work contains the results of the first part of that investigation.

As a result of a preliminary analysis of the present elastic data,[7] two of the present authors have developed an interpretation of the elastic scattering of composite projectiles at intermediate energies[8] which emphasizes the refractive aspects of the process rather than the more commonly discussed diffractive aspects; they also outlined criteria for the incident energy and angular range of measurements required to eliminate the discrete ambiguities in the optical potentials for such projectiles.[9] The criteria are reviewed here briefly, and the elastic scattering data which led to their formulation are discussed is some detail. In Sec. III B the size or A dependence of the required incident energy is demonstrated through a comparison of the ^{58}Ni and ^{208}Pb elastic scattering results. Also, by examining the effective optical potentials (nuclear plus Coulomb plus centrifugal), we are able to demonstrate explicitly why the phase-